King's Research Portal

DOI:
10.1016/j.celrep.2019.04.076

Document Version
Peer reviewed version

Link to publication record in King's Research Portal

Citation for published version (APA):
Evans, R., Flores-Borja, F., Nassiri, S., Miranda, E., Lawler, K., Grigoriadis, A., Monypenny, J., Gillett, C., Owen, J., Gordon, P., Male, V., Cheung, A., Noor, F., Barber, P., Marlow, R., Francesch-Domenech, E., Fruhwirth, G., Squadrito, M., Vojnovic, B., ... Ng, T. (2019). Integrin-mediated macrophage adhesion promotes lymphovascular dissemination in breast cancer. *Cell Reports*, *27*(7), 1967-1978.e4. https://doi.org/10.1016/j.celrep.2019.04.076

Citing this paper
Please note that where the full-text provided on King's Research Portal is the Author Accepted Manuscript or Post-Print version this may differ from the final Published version. If citing, it is advised that you check and use the publisher's definitive version for pagination, volume/issue, and date of publication details. And where the final published version is provided on the Research Portal, if citing you are again advised to check the publisher's website for any subsequent corrections.

General rights
Copyright and moral rights for the publications made accessible in the Research Portal are retained by the authors and/or other copyright owners and it is a condition of accessing publications that users recognize and abide by the legal requirements associated with these rights.

•Users may download and print one copy of any publication from the Research Portal for the purpose of private study or research.
•You may not further distribute the material or use it for any profit-making activity or commercial gain
•You may freely distribute the URL identifying the publication in the Research Portal

Take down policy
If you believe that this document breaches copyright please contact librarypure@kcl.ac.uk providing details, and we will remove access to the work immediately and investigate your claim.

Download date: 03. Jan. 2025

Integrin-mediated macrophage adhesion promotes lymphovascular dissemination in breast cancer

Rachel Evans[1,11]†*, Fabian Flores-Borja[2]†††, Sina Nassiri[3], Elena Miranda[4], Katherine Lawler[1,5], Anita Grigoriadis[2], James Monypenny[1], Cheryl Gillet[6,7], Julie Owen[6,7], Peter Gordon[2], Victoria Male[2]††, Anthony Cheung[2], Farzana Noor[2], Paul Barber[1,11], Rebecca Marlow[2], Erika Francesch-Domenech[2], Gilbert Fruhwirth[8], Mario Squadrito[3], Boris Vojnovic[9], Andrew Tutt[2], Frederic Festy[10], Michele De Palma[3], Tony Ng[1,2,11*]

[1]Richard Dimbleby Department of Cancer Research, Randall Division & Division of Cancer Studies, Kings College London.

[2]Breast Cancer Now Research Unit, King's College London, Guy's Hospital, London.

[3] Swiss Institute for Experimental Cancer Research (ISREC), School of Life Sciences, École Polytechnique Fédérale de Lausanne (EPFL), Switzerland

[4]Pathology Core Facility, University College London Cancer Institute, London, WC1E 6DD.

[5]Institute for Mathematical and Molecular Biomedicine, King's College London.

[6]King's Health Partners Cancer Biobank, King's College London.

[7]Research Oncology, Division of Cancer Studies, Guy's Hospital, King's College London.

[8]Division of Imaging Sciences and Biomedical Engineering, King's College London.

[9]Gray Laboratories, Department of Oncology, Oxford University.

[10] Tissue engineering and Biophotonics, Guy's Medical School Campus, King's College London.

[11]UCL Cancer Institute, University College London.

† Current address: Cancer Institute, University College London.

†† Current address: Division of Infection and Immunity, Institute of Immunity and Transplantation, University College London.

††† Current address: Centre for Immunobiology and Regenerative Medicine, Barts & The London School of Medicine and Dentistry, Queen Mary University of London

***Correspondence should be addressed to:** Prof Tony Ng (Lead Contact) and Dr Rachel Evans

e-mail: tony.ng@kcl.ac.uk or rachel.evans@ucl.ac.uk

Conflict of interest statement: The authors have declared that no conflict of interest exists.

SUMMARY

Lymphatic vasculature is crucial for metastasis in triple-negative breast cancer (TNBC); however, cellular and molecular drivers controlling lymphovascular metastasis are poorly understood. We define a macrophage-dependent signaling cascade that facilitates metastasis through lymphovascular remodeling. TNBC cells instigate mRNA changes in macrophages resulting in β4 integrin-dependent adhesion to the lymphovasculature. β4 integrin retains macrophages proximal to lymphatic endothelial cells (LECs), where release of TGFβ1 drives LEC contraction via RhoA activation. Macrophages promote gross architectural changes to lymphovasculature by increasing dilation, hyperpermeability and disorganization. TGFβ1 drives β4 integrin clustering at the macrophage plasma membrane further promoting macrophage adhesion, demonstrating dual functionality of TGFβ1 signaling in this context. β4 integrin expressing macrophages were identified in human breast tumors and a combination of vascular-remodeling macrophage gene signature and TGFβ signaling scores correlates with metastasis. We postulate that future clinical strategies for patients with TNBC should target crosstalk between β4 integrin and TGFβ1.

Key Words: Lymphovasculature, macrophages, cancer, remodeling, adhesion, α6β4 integrin, TGFβ1, RhoA.

INTRODUCTION

Tumor cells establish complex interactions with cells within their microenvironment that determine malignancy progression (Balkwill et al., 2012). Tumor cell dissemination can occur through blood or lymphovasculature, however targeting blood vasculature has limited clinical efficacy when lymphatic dissemination is prevalent (Wong and Hynes, 2006).

Breast cancer is divided into subtypes based on histopathological features and gene signatures (Gazinska et al., 2013).Triple-negative breast cancer (TNBC) is characterized by a lack of druggable targets, is a highly metastatic and associated with dismal prognosis (Gazinska et al., 2013, Dent et al., 2007). The prognostic significance of lymphangiogenesis in TNBC is under debate. However, invasion into lymphatic vessels correlates with poor prognosis suggesting that targeting existing lymphatic vessel network could provide an effective treatment strategy (Choi et al., 2005, Mohammed et al., 2011, Mohammed et al., 2007, Liu et al., 2009).

The relationship between tumor and immune cells is often bidirectional and involves both tumor-promoting and antagonizing mechanisms (Pollard, 2004, Quail and Joyce, 2013). Among innate immune cells, macrophages have been implicated in the promotion of tumor progression and, in particular, breast cancer metastasis (Condeelis and Pollard, 2006, Kitamura et al., 2015, Pollard, 2004, Harney et al., 2015). However, it remains unclear how certain subsets of tumor-associated macrophages (TAMs) influence breast cancer metastasis spatially, temporally and at a molecular level.

The integrin family are adhesion receptors of paramount importance for immune cell adhesion and migration during inflammatory processes (Evans et al., 2009). Their ability to form adhesive contacts is regulated by soluble factors, as part of the chemoattractant-adhesion crosstalk that causes a combination of changes in integrin conformation and clustering on the plasma membrane (PM) that regulate downstream signaling (Hynes, 2002). In malignancy, many integrins common in epithelial cells are also present in solid tumors and some, such as αvβ3 and α5β1 are specifically upregulated in cancer (Desgrosellier and Cheresh, 2010). Tumor-expressed integrins affect tumor cell migration, proliferation, survival and anchorage to the extracellular matrix. Endothelial cell-expressed integrins are implicated in angiogenesis, lymphangiogenesis and vascular remodeling (Avraamides et al.,

2008). While the importance of integrins with respect to maintaining a pro-tumoral immune microenvironment in solid tumors is not well defined, in chronic lymphocytic leukemia, impaired integrin signaling in non-leukemic T cells changes the immune microenvironment to be more immunosuppressive which may facilitate malignancy progression (Ramsay et al., 2013).

We seek to identify the role of tumor-associated macrophages (TAMs) in regulating existing lymphovasculature in TNBC where lymphatic dissemination is not a direct result of lymphangiogenesis.

We propose that macrophages have an important role in controlling established tumoral lymphatic networks in TNBC, and that lymphatic dissemination of cancer cells is facilitated by a cascade of signaling events initiated by integrin-mediated adhesion of macrophages at the sites of lymphatic vessels.

RESULTS

Lymphovascular macrophages in TNBC mouse models are retained through binding of β4 integrin to laminin-5. To identify endogenous macrophages with respect to lymphatic vasculature in murine TNBC tumors we scored F4/80+Tie2+ macrophages within podoplanin+ lymphovasculature across multiple fields of view (FOV) from 4T1.2 and BLG-Cre;Brca1$^{f/f}$,p53$^{+/-}$ TNBC models (Molyneux et al., 2010, Melchor et al., 2014) (Figure 1 A and B). The Tie2-expressing macrophage (TEM) subset is associated with angiogenesis and lymphatic development (De Palma et al., 2007, De Palma et al., 2005, Gordon et al., 2010). Lymphovascular associated macrophages expressing Tie2 have recently been reported in a small breast cancer cohort (Bron et al., 2016). In 4T1.2 tumors we found a mean value of 6.3 F4/80+Tie2+ macrophages within podoplanin+ vasculature (versus 1.7 in podoplanin- regions) per FOV. In BLG-Cre;Brca1$^{f/f}$,p53$^{+/-}$ tumors we observed 8.8 F4/80+Tie2+ macrophages in podoplanin+ vasculature (versus 2.0 in podoplanin-regions) per FOV. Therefore F4/80+Tie2+ macrophages are enriched in lymphovascular regions in murine TNBC models.

The β4 integrin subunit is a transmembrane glycoprotein associating exclusively with α6 integrin subunit. α6β4 integrin is expressed predominantly on epithelial and endothelial cells and binds to laminins to form adhesion complexes, hemidesmosomes (Stewart and O'Connor, 2015). Microarray analysis of endogenous macrophages co-cultured with 4T1.2 tumor cells showed mean 1.8-fold upregulation of β4 integrin at the RNA level compared with non-educated endogenous macrophages and that the RAW264.7 macrophage cell line similarly exhibited mean 1.58-fold increase in β4 integrin levels compared to endogenous macrophages (Figure 1 C and data published in Array Express: MTAB-4064).

4T1.2 tumors were excised and disaggregated at day 10. Within 4T1.2 tumors we defined a population of macrophages as CD45^{+}Ly6G^{-}CD31^{-}CD11b^{+}Tie2^{+}β4 integrin^{+} (Figure 1 D).

The influence of tumor education on macrophage adhesion to β4 integrin ligand, laminin-5, was investigated. Tumor-educated endogenous macrophages displayed increased adhesion to laminin-5 (30.7 ± 7.2% to 81.7 ± 13.2 % adherent cells on 0.5 μM laminin-5; Figure 1 E). As laminin-5 is reportedly localized in areas with high blood vessel density we investigated if laminin-5 was also in areas of

lymphovasculature. 4T1.2 tumor tissue analysis showed laminin-5 furnished around podoplanin+ lymphovasculature (Figure 1 F). In addition we observed macrophages expressing α6β4integrin in lymphovascular regions (Figure 1G).

To study β4 expression in vivo we used primary 4T1.2 tumor sections stained with Lyve1-Cy3 and β4 integrin-Cy5. Tissues were imaged using a protocol involving laser photobleaching to remove autofluorescence. Our methodology reveals β4 integrin throughout the tumor; however within lymphatic vessels there is differential distribution of β4 integrin with relative increases in β4 accumulation observed in lymphovascular areas proximal to Lyve1+ lymphatic endothelial cells (LECs) (white arrow). Additionally there were lymphovascular areas with increased localized Pearson coefficient suggesting LECs and β4 integrin-expressing macrophages in close contact (blue arrow) (Figure 1 H) (mean colocalization coefficient of 4.094 ± 0.8146).

TAMs drive disorganized and hyperpermeable lymphatic architecture and contact between macrophages and LECs results in RhoA-dependent contraction. We used a mammary image window (MIW) subcutaneously implanted over a 4T1.2-mCherry tumor (Kedrin et al., 2008) (Figure 2A). Injection of 76kDa dextran-FITC allowed visualization of lymphatic vasculature. Using multiphoton microscopy we observed that within the tumor, lymphatic vessels leaked dextran dye across the FOV (left panel) suggesting high levels of vessel permeability, however in more distal regions, lymphatic vessels had a distinct structure and 4T1.2-mCherry intra-lymphatic tumor cells could be seen within vessels, suggesting ongoing metastasis (middle and right panel respectively). To understand how increasing tumor-associated macrophages could phenotypically influence lymphatic vasculature we studied permeability of lymphatic vessels from 4T1.2 tumor-bearing mice given intermittent bolus of RAW264.7 macrophages during tumor development. Both RAW264.7 macrophages and the 4T1.2 tumor line are derived from a BALB/c genetic background allowing us to investigate effects of elevated macrophage numbers on tumor progression in vivo using a syngeneic model of TNBC.

To quantify lymphatic vessel permeability in vivo we adapted a protocol previously used in angiogenesis studies (Finsterbusch et al., 2014). Using a subcutaneous injection of Evans Blue dye, we quantified permeability of the tumoral lymphatics.

Tumors with elevated macrophages contained hyperpermeable lymphatic vessels with an increase in mean OD per g from 0.7812 ± 0.2956 to 2.290 ± 0.5160 when compared to PBS-treated control, suggesting a facilitated pathway between the primary tumor and lymphatic vasculature (Figure 2 B).

To understand effects of elevated macrophages on tumoral lymphatic vessel architecture we stained tumour sections from mice treated with PBS or RAW264.7 macrophages with the lymphatic vessel markers, Lyve1 and podoplanin (Figure 2 C and SI 1 A&B) demonstrating both lymphatic markers gave a similar staining distribution. Typical sections from PBS treated mice showed small well-formed vessels towards the tumor periphery or within the peri-tumoral areas with a mean diameter of 13.66 μm ± 1.295. This was in contrast to RAW264.7 treated mice that had larger vessels with a mean diameter of 48.00 μm ± 6.065 indicating increased vessel dilation (SI 1 C).

To quantify changes in lymphatic architecture in tumors with elevated levels of macrophages we blindly scored lymphovasculature for disorganization based on the following criteria. Smaller vessels with a clear lumen were given low scores (0 and 1) compared to larger disorganized vessels with unclear borders (2 and 3). PBS treated tumors had a mean disorganization score of 0.25 ± 0.16 and 1.6 ± 0.33 compared to 1.8 ± 0.29 and 2.5 ± 0.17 for tumors treated with RAW264.7 macrophages (Figure 2 C).

To further investigate whether macrophages were sufficient to induce a disorganized lymphatic phenotype we ablated endogenous macrophages using clodronate-containing liposomes post-establishment of 4T1.2 tumors. Endogenous macrophages were reconstituted post-clodronate treatment with non-educated bone marrow macrophages (BMM) or tumor-educated BMM for 48 hours (Figure 2 Di). The extent of lymphatic disorganization in the 4T1.2 primary tumors was greater after reconstitution with endogenous tumor-educated BMM compared to non-educated BMM (0.333 ± 0.3 to 2 ± 0.29; Figure 2 Dii, iii). These results demonstrate that the presence of tumor-associated macrophages results in a disorganized lymphatic vasculature around the primary tumor, that the extent of disorganization is related to overall macrophage levels and that this occurs at an early time point in tumor development (day 10-14).

To investigate how tumor-associated macrophages affect lymphatic endothelia we added endogenous macrophages to monolayers of primary LECs isolated from BALB/c mice (Figure 2 E). Primary lymphatic endothelial cells had a mean spread area of 1132μm^2 ± 247.9 which reduced slightly to 808.6 μm^2 ± 185.9 after addition of endogenous uneducated macrophages but dramatically reduced to 324.1 μm^2 ± 76.43 with tumor-educated macrophages and 473.7 μm^2 ± 92.8 with ex vivo tumor-associated macrophages ($CD45^+Ly6G^-CD31^-CD11b^+$). Similar LEC contraction occurred when the murine lymphatic endothelial cell line, SV-LECs (Ando et al., 2005) were grown as a monolayer and endogenous macrophages (SI 1 D) or RAW264.7 macrophages added (Figure 2 Fi). SV-LEC contraction occurred with area reducing from 835.9 μm^2 ± 72.32 to 380.5 μm^2 ± 40.82 and 632.5 μm^2 ± 83.0 to 82.67μm^2 ± 14.38 respectively. In addition area of SV-LECs was quantified with and without contact with RAW264.7 macrophages. SV-LEC contraction was only observed when direct contact between the 2 cell types occurred (436.4 μm^2 ± 63.3 to 116.2 μm^2 ± 34.6) (Figure 2 Fii). Collectively our evidence suggests direct contact between tumor-associated macrophages and lymphatic endothelial cells is required for contraction events to occur.

RhoA regulates many events in blood vessel-specific endothelial cells during angiogenesis such as motility, proliferation and permeability (Bryan et al., 2010). We sought to test whether RhoA regulates contraction events observed in LECs. SV-LECs were transiently transfected with the GFP- and mRFP-expressing RhoA Raichu biosensor (Heasman et al., 2010, Makrogianneli et al., 2009, Yoshizaki et al., 2003) that allows measurement of the fluorescent lifetime decay (Tau) when FRET occurs between the GFP and mRFP upon RhoA activation. After SV-LEC transfection, non-educated or tumor-educated endogenous macrophages were added to SV-LECs for 24 h. The fluorescence lifetime of the Raichu probe (expressed exclusively in the SV-LECs) was measured using multiphoton microscopy. SV-LEC co-culture with tumor-educated macrophages led to a reduction in donor fluorescent lifetime (Tau) of the biosensor from 1.797 ns ± 0.0252 to 1.622 ns ± 0.0338, indicating increase in FRET between the GFP and RFP terminal fluorophores and consequently an increase in RhoA activity (Figure 2 G). No change in Tau was observed when SV-LECs were co-cultured with non-educated endogenous macrophages (Figure 2 G ii). These results demonstrate RhoA activity

increases during LEC contraction and that this only occures in the presence of tumor-educated macrophages in contact with lymphatic endothelia.

Lymphatic endothelial cell contraction is dependent on TGFβ1 release from tumor-educated macrophages

TGFβ receptor ligation in fibroblasts results in RhoA activation (Fleming et al., 2009). We investigated release of active TGFβ1 and TGFβ2 isoforms from non-educated and tumor-educated macrophages by ELISA (Figure 3 A). TGFβ1 levels increased from 2600 pg to 4400 pg in tumor-educated endogenous macrophages (increase in optical absorbance at 450 nm from 1.286 ± 0.07119 to 2.585 ± 0.1077). In contrast TGFβ2 levels were not significantly changed. While TGFβ is present throughout the tumor microenvironment, membrane-bound TGFβ can have a potent effect on downstream signaling though increasing the concentration gradient of this molecule (Savage et al., 2008). Our data showed 4T1.2 education of endogenous macrophages significantly increased the levels of plasma membrane bound TGFβ1 (Figure SI 2 A) allowing stringent spatial control of downstream signaling events.

To test the hypothesis that macrophage-released TGFβ1 was responsible for LEC contraction we investigated the effect of a TGFβ-receptor inhibitor, SB-431542 (Inman et al., 2002) (Figure SI 2 B). As expected, RAW264.7 macrophages alone induced LEC contraction (950.6 μm^2 ± 129.9 to 335.8 μm^2 ± 38.23); however this did not occur in the presence of SB-431542 or when TGFβ1 or β4 integrin were transiently knocked down in RAW264.7 macrophages, demonstrating that the presence of β4 integrin and TGFβ in macrophages or TGFβ receptor ligation on LECs was sufficient to prevent contraction (Figure 3 B and SI 2 C & D).

The role of macrophage-released TGFβ1 on lymphovascular disorganization was investigated in vivo. A stable knockdown of TGFβ1 was generated in RAW264.7 macrophages using lentiviral shRNA (Figure SI 2 E). Similar to our previous in vivo studies, macrophages were administered intravenously throughout tumor development. After 2 weeks growth, tissue sections were stained for Lyve1 and podoplanin. The extent of lymphatic disorganization in tumors with RAW264.7-TGFβ1 knockdown compared to RAW264.7-NTC was blindly scored in Lyve1/podoplanin stained tissues as before. Our results show that absence of TGFβ1 in RAW264.7 macrophages was sufficient to significantly decrease extent of

lymphatic disorganization observed compared to RAW264.7-NTC macrophages (1.8 ± 0.16 to 1.1 ± 0.18) (Figure 3 C) and that these changes were evident at an early time-point.

To functionally associate macrophage-released TGFβ1 to structural changes in the lymphatic endothelium in vivo we quantified levels of phospho-myosin light chain (pMLC) in LECs adjacent to macrophages. Since RhoA activity is high in contracting LEC and active RhoA phosphorylates MLC, pMLC can be used as a read-out of LEC contractility in cells proximal to lymphatic-associated macrophages. We observed that when mice were injected with RAW264.7-TGFβ1 knockdown compared to RAW264.7-NTC, there was significant reduction in pMLC levels in lymphatic vasculature adjacent to RAW264.7 macrophages when TGFβ1 was absent (1.97 $x10^6$ ± 401151 to 6.56 $x10^5$ ± 187133) (Figure 3 D).

TGFβ1 controls β4 clustering at the macrophage plasma membrane

We studied the effect of TGFβ1 on the phenotypic functionality of macrophages by quantifying spreading response of macrophages. There was clear reduction in cell spreading when TGFβ1 was knocked down in RAW264.7 macrophages compared to the non-targeted control counterpart (235.2 μm^2 ± 41.06 to 91.91 μm^2 ± 11.62) (Figure 3 E). To understand how TGFβ1 could control macrophage spreading we investigated the effect of TGFβ1 on β4 expression. Since integrins can be constitutively expressed on the cell surface we sought to study the plasma membrane distribution of β4 integrin using structured illumination microscopy in RAW264.7-TGFb1shRNA versus RAW264.7-NTC. Our results clearly show that while there may be small differences in the overall amount of β4 integrin expressed on the cell surface (SI 3 A & B), the size of integrin clusters which can form firm adhesive contact with integrin ligand are significantly reduced when TGFβ1 is absent (1.97 μm^2 ± 0.12 to 1.559 μm^2 ± 0.0.07; Fig 3 Fi and ii). These results collectively indicate that TGFβ1 has both a paracrine role in controlling the lymphatic endothelium and an autocrine role in regulating β4 activity in tumor-educated macrophages.

β4 integrin+ macrophages and lymphatic remodeling are associated with TGFβ signaling and adverse outcome in TNBC patients

To establish that human macrophages express ITGB4 RNA (β4 integrin) we performed an analysis of a compendium of data composed of macrophages from in vitro and in vivo data sets. We observed that ITGB4 is expressed in both human and mouse total macrophages (Figure 4 A & SI 4 A). From the same compendium a correlation between ITGB4 expression and signaling downstream of TGFβ1 was established (Figure 4 B). Single-cell transcriptome analysis of non-tumor cells isolated from primary breast tumors revealed that TAMs expressed high levels of ITGB4 compared to other non-tumor cells within the tumor microenvironment (Figure 4 C). To identify patients that may have enrichment of macrophages capable of lymphovascular remodeling we used a gene signature containing genes enriched in Tie2 expressing macrophages (TEMs) (Pucci et al., 2009) in a cohort of 122 TNBC gene expression patterns (Gazinska et al., 2013). We plotted the activation score of the TEM gene signature against the TGFβ signaling pathway for each tumor, and observed enrichment of patients with distant metastasis when both of these gene signatures were present in the primary tumor (Fig 4D). Kaplan-Meier plots also showed a significant reduction in distant metastasis free survival (DMFS) in patients classified as having a high TEM/TGFβ activation score (Figure 4E). To investigate the presence of lymphatic-associated macrophages in breast cancer patients, samples from 20 patients were used. Of these patients, 10 were previously characterized as having lymphatic vessel invasion (LVI) and the remaining 10 did not have LVI. To assess macrophage localization with respect to lymphatic vasculature, we dual stained sections with an antibody against CD14 and podoplanin (Figure 4F). The sections were scored for presence of CD14+ macrophages within or proximal to lymphatic vasculature. In our cohort of 20 patients, all samples exhibited some degree of CD14 and podoplanin positivity. Six cases (30%) had macrophages associated with lymphatic vessels and of these, 4 were shown to be positive for LVI. In this small study, our results suggests that 67% of patients with lymphatic-associated macrophages also have LVI. In a separate small patient cohort (8 patients), we demonstrated CD68+ macrophages expressing β4 integrin (ITGB4) in close proximity to podoplanin+ vessels using consecutive paraffin-embedded sections (Figure 4 G&H). We quantified CD68+ITGB4+ macrophages per mm^2 and saw an association between CD68+ITGB4+ macrophage score and lymph node positivity in individual patients (SI 4 B). Future studies will endeavor to repeat this

small study in a larger patient cohort to investigate whether this relationship is statistically significant. The combination of our data suggests that β4 integrin-expressing lymphovascular macrophages may be driving LVI and subsequent metastasis to lymph nodes via the lymphatic remodeling signaling cascade.

DISCUSSION

This study demonstrates how crosstalk between a previously unreported tumor-infiltrating myeloid subpopulation and existing lymphatic vasculature can promote metastasis through quantifiable architectural changes in lymphatic vessels. We identified a population of β4 integrin-expressing macrophages that drive lymphatic remodeling through TGFβ signaling and are associated with adverse pathological response in TNBC patients.

Our study uses both endogenous bone marrow macrophages and the RAW264.7 macrophage cell line, which is strain-matched to the lymphotropic tumor cell line, 4T1.2. Through intravital imaging and ex vivo tissue analysis, our TNBC model allows us to probe the relationship between the tumor lymphatic vasculature and macrophages in vivo and directly translate these phenotypic observations into in vitro assays for mechanistic studies. We then directly assess the prognostic significance of the key molecules in the lymphatic signaling cascade in predicting adverse pathological outcome for a cohort of TNBC patients. In breast cancer samples previously characterized for LVI we identify lymphatic-associated macrophages in approximately a third of samples and show that LVI was present in the majority of these cases. We identify α6β4-expressing macrophages proximal to lymphatic endothelium in breast cancer samples, and demonstrate that in patients with a larger α6β4-expressing macrophage infiltrate, there is a trend towards sentinel lymph node metastasis. Our data suggest that α6β4-expressing macrophages may drive metastasis via the lymphovascular route in human breast cancer.

Our study reveals that macrophages are retained in lymphatic endothelium in a TNBC model through upregulation of β4 integrin on tumor-educated macrophages. While the adhesion receptor α6β4 integrin is ubiquitously expressed in early breast cancer (Diaz et al., 2005), transcriptome analysis of breast cancer patient samples revealed a correlation between expression levels and prognosis (Lu et al., 2008). Through analysis of β4 integrin at transcriptome and protein level we demonstrate a population of endogenous macrophages that express β4 integrin and are adherent to laminin-5 in lymphovascular areas. Collectively our data suggest that β4 integrin acts to ensure that tumor-infiltrating macrophages are in a prime location for sustained interaction with lymphatic endothelial cells.

We have defined dual functionality of TGFβ1 where it can affect signaling within tumor-associated macrophages and LECs. Firstly, we show that TGFβ1 is required for α6β4 integrin clustering at the macrophage plasma membrane. Integrin clustering can positively regulate levels of cell adhesion rapidly in response to soluble stimuli (Hynes, 2002). TGFβ has previously been demonstrated to control α6β1 and α6β4 integrin clustering in HER2-overexpressing mammary tumor cells (Wang et al., 2009). Here we describe TGFβ1 dependent β4 integrin clustering in macrophages which control the macrophage spreading response necessary for TAM adhesion at the site of lymphatic vasculature.

Secondly, TGFβ1 acts in a paracrine manner to activate RhoA in LECs lining the lymphatic vessel demonstrated through RAICHU-FLIM technology (Heasman et al., 2010, Makrogianneli et al., 2009, Vega et al., 2011). Our study shows that signaling within LECs in contact with TAMs drives LEC contraction, which correlates to gross architectural changes and hyperpermeability of the lymphatic vessel network that could actively facilitate metastasis. We have previously demonstrated the activation of RhoGTPases by integrin signaling *in cis* (on the immune cells that are triggered by adhesion processes (Makrogianneli et al., 2009, Carlin et al., 2011, Heasman et al., 2010, Ramsay et al., 2013). Our current study indicates this phenomenon can also occur *in trans* i.e. activation of RhoGTPases in the endothelial cells that are contacted by the adherent macrophages, through the expression of factors such as TGFβ1.The role of macrophage-released TGFβ1 in vivo is shown to have an effect on the RhoA pathway in proximal LEC and a concomitant role in lymphovasculature disorganization.

In summary, this study identifies an alternative macrophage-mediated signaling pathway involved in promotion of lymphatic metastasis. Our work emphasizes the importance in considering crosstalk between macrophages and the lymphatic vessel network in TNBC, where aggressive tumor growth and rapid metastasis often mean a poor outcome. We hope this study will guide future endeavors to focus on therapeutically targeting the lymphatic remodeling signaling cascade in TNBC disease progression.

Acknowledgments: We thank Cancer Research UK King's Health Partners Centre at King's College London, Nikon Imaging Centre, King's College London; Mathew Smalley for tumor tissue from BLG-Cre;Brca1$^{f/f}$,p53$^{+/-}$ mice; Steven Alexander for murine SV-LEC line; UCL Pathology core facility; Kalnisha Naidoo for advice; James Arnold, Victoria Sanz-Moreno, Hellmut Augustin and Anne Ridley for reviewing the manuscript.

Author contributions: R.E conceptualized the study, designed, performed and analysed experiments, and wrote the manuscript; F.FB performed FACS acquisition and analysis, assisted with in vivo experiments , assisted with experiment analysis and assisted with writing the manuscript; S.N performed gene analysis on macrophage populations and assisted with writing the manuscript; E.M. stained, quantified and analysed CD68+ITGB4+ patient tissues. K.L. performed in vitro macrophage gene array analysis, and assisted with writing the manuscript; A.G. analysed TNBC gene expression data, and assisted with writing the manuscript;, J.M. assisted with in vivo experiments and writing the manuscript; C.G. and J.P. selected, stained and analysed breast cancer sections; P.G. assisted with in vivo experiments; V.M. designed the lymphatic disorganization scoring assisted with data analysis; A.C assisted with analysis; F.N assisted with antibody optimisation; P.B. gave technical advice on analysing FRET/FLIM data; R.M and E. F-D performed tumor transplantation; G.F and B.V. gave technical advice on intravital imaging; M.L.S contributed reagents; A.T. contributed to clinical translation and reviewed the manuscript; F.F. wrote the colocalization software, analysed colocalization data; M.DP contributed reagents and reviewed the manuscript; T.N. provided funding, contributed to clinical translation and assisted with writing the manuscript.

Funding: This work was funded by Cancer Research UK Health Partner's Centre at KCL, KCL/UCL Comprehensive Cancer Imaging Centre and Breakthrough Breast Cancer (recently merged with Breast Cancer Campaign forming Breast Cancer Now).

Abbreviations:

BMM: Bone marrow macrophage

eBMM: Tumor-educated bone marrow macrophage

MIW: Mammary imaging window

TAM: Tumor-associated macrophage

TNBC: Triple-negative breast cancer

SIM: Structured illumination microscopy

ITGB4: β4 integrin

LVI: Lymphatic vessel invasion

LN: lymph node

FOV: Field of view

Titles and legends to figures

Figure 1. Lymphovascular macrophages in TNBC mouse models are retained through binding of β4 integrin to laminin-5. Tumor sections from 4T1.2 (A) and BLG-Cre;Brca1$^{f/f}$,p53$^{+/-}$ (B) stained with F4/80-FITC, podoplanin-AF555 and Tie2 -Cy5 conjugated antibody. F4/80+Tie2+ macrophages within podoplanin+ areas versus those in other areas quantified per field of view (FOV). Vessel lumen outlined, arrow shows a macrophage within a podoplanin+ area. Images acquired with x40 air objective, scale bar 100 μm (main image), 25 μm (zoomed inset). (C) Array-derived expression profile of β4-integrin (Itgb4) across samples. Barplot shows $\log_2$ fold-change of normalized expression value for β4 integrin (ratio of the median value of probe in BMM samples). (D) Day 12 4T1.2 tumors were disaggregated. Tie2 and β4 integrin FMO controls shown in 2 left panels. Right dot plot and histogram depict β4 integrin expressing macrophages from representative 4T1.2 tumor (n = 8). (E) BMM co-cultured alone/with 4T1.2-GFP cells plated on laminin-5. % adherent cells quantified in triplicate (n = 2). 4T1.2 tumor sections stained with (F) laminin-5-Dylight488 and podoplanin-AF555 (G) Lyve1-Cy3; F4/80-FITC and β4 integrin-cy; inset shows F4/80+β4 integrin+ macrophages around lymphatic endothelium. (H) Stained sections (Lyve1-Cy3 and β4 integrin-Cy5) imaged using a custom-built microscope (x20 air obj). Area of distinct β4 integrin and Lyve1 within lymphatic vessel (white arrow) and area of close contact between β4 integrin and Lyve1 (blue arrow). Scale bar, 50 µm (main panels), 25 µm in (inset).

Figure 2. TAMs drive dilated, hyperpermeable and disorganized lymphatic architecture through LEC RhoA activation. (A) i) Mouse with mCherry-tagged 4T1.2 tumor and implanted mammary imaging window (MIW) at day 10-14. ii) Lymphatic vessels (green) surrounding tumor (red, left panel; lymphatic vessels (green) distal to main tumor bulk (red, middle panel); lymphatic vessel (green) with tumor cells (red) within vessel (right panel). Scale bar, 100 μm. (B) 4T1.2 tumor-bearing mice treated with PBS or RAW264.7 macrophages over 3 weeks. 1% Evans Blue dye stained lymphatics in vivo. Lymphatic permeability calculated as optical density per gram tumor. Data represent means ± SEM, significance determined using unpaired t-tests (**$p<0.01$). (C) i) Lymphatic vessels within tumors from mice treated with PBS or RAW264.7 macrophages stained with Lyve1-Cy3 or podoplanin-AF555 (red), and blindly scored for disorganization. Scale bar, 50 µm ii) Four FOV in

4 PBS-treated and 4 RAW264.7 macrophage-treated tumor samples scored blindly for disorganization. Data represent means ± SD, significance determined using unpaired t-tests (***p<0.001) (D) i) Timeline depicting clodronate-containing liposome protocol. ii) Tumor sections from clodronate-treated mice reconstituted with PBS, BMM or BMM stained with Lyve1-Cy3 or podoplanin-AF555 (red). Lymphatic disorganization within tumors from 6 mice quantified from > 3 FOV per mouse from Lyve1 stained sections. Data represent means ± SD, significance determined using unpaired t-tests (**p<0.01). (E) Primary LEC cultured alone, with BMM, tumor-eBMM or TAM. LEC stained with podoplanin-AF555 and macrophages stained with F4/80-FITC. Confocal microscopy (x40 air obj) used to quantify area of LEC from 3 FOV (n = 2). Scale bar, 10 µm. (F) i&ii) Monolayer of SV-LECs (cell tracker green (CMFDA)) with RAW264.7 macrophages (cell tracker orange (CMTMR)) after 24 h. Area of SV-LECs measured using ImageJ software. Data represent means ± SEM; significance determined using unpaired t-tests (**p<0.01). Scale bar, 25 µm. (G)i) SV-LECs transfected with RhoA Raichu biosensor (Raichu R/G) or RhoA-GFP as a control. Transfected SV-LECs cultured alone or with BMM/eBMMfor 24 h. ii) Multiphoton microscopy used to determine fluorescence lifetime (Tau (ns)) of SV-LECs transfected with RhoA-GFP or RhoA Raichu biosensor. Data represent means ± SD, significance determined using unpaired t-tests (**p<0.01).

Figure 3. Macrophage-expressed TGFβ1 regulates β4 integrin clustering on the macrophage plasma membrane and is required for LEC contraction. (A) Bone marrow macrophages cultured alone (BMM) or with 4T1.2 cells (BMM co-culture). Supernatants probed for i) TGFβ1 and ii) TGFβ2 by ELISA. Data represent means ± SD and significance determined using unpaired t-tests (***p<0.001). (B) SV-LECs grown as monolayers. Tumor-educated RAW264.7 macrophages (eRAW) added plus DMSO control /10 µM SB-431542. After 24 h, SV-LEC areas were quantified. Data represent means ± SD, significance determined using unpaired t-tests (****p<0.0001). (C) Tumor-bearing mice injected with RAW264.7-NTC or RAW264.7-TGFβ1 knockdown until d 14. Tumors sections stained with podoplainin-AF555 or Lyve1-Cy3 and Lyve1+ vessels blindly scored for lymphatic disorganization (*p<0.05). Scale bar, 50 µm. (D) Tumor-bearing mice injected with RAW264.7-NTC or RAW264.7-TGFβ1 until d 21. Tumor sections were stained with F4/80-FITC, pMLC (and Rabbit-Cy3 secondary antibody) and podoplanin-Cy5. F4/80+ cells within

podoplanin+ regions were identified and a 65 μm^2 ROI was identified (white circles) where fluorescence intensity of pMLC signal was quantified. Scale bar, 50 μm (4 FOV from n = 2 tumors from each condition). Data represent means ± SD, significance determined using unpaired t-tests (**p<0.01). (E) RAW264.7-NTC or RAW264.7-TGFβ1 macrophages area measured by confocal microscopy. Data represent means ± SD, significance determined using unpaired t-tests (**p<0.01). (F) RAW264.7-NTC or RAW264.7-TGFβ1 stained with anti-β4 integrin-AF647 and imaged using structured illumination microscopy (Nikon x100 oil objective). Focal adhesion area determined using ImageJ on thresholded images. Data represent means ± SD, significance determined using unpaired t-tests (**p<0.01). Scale bar, 10 µm; 1µm (inset).

Figure 4. β4 integrin-expressing macrophages and lymphatic remodeling associated with TGFβ signaling and adverse outcome in TNBC patients. (A) ITGB4 expression in human macrophages. Y-axis indicates normalized expression on log2 scale. Red line indicates median expression of all genes. Raw gene counts obtained from the ARCHS4 database. (B) Correlation between ITGB4 expression and enrichment of TGFβ signaling in human macrophages (Spearman rho = 0.26; p<0.001. X-axis indicates normalized expression on the log2 scale. Y-axis indicates ssGSEA enrichment scores computed for the TGFβ hallmark gene set obtained from MSigDB data base. Red curve indicates loess fit. Association strength quantified using Spearman correlation coefficient. Raw gene counts obtained from the ARCHS4 database. (C) Expression of ITGB4 in scRNAseq data of primary breast cancer (GSE75688). Data reported as log2(TPM+1). (D) Activation score of TEM gene signature and TGFβ signaling shown. Red and green dots indicate TNBC with/without distant metastasis respectively. Enrichment of TNBC with distant metastasis in the top right quadrant established by hypergeometric testing. (E) Kaplan-Meier survival curves showing distant metastasis free survival in TNBC. Stratification based on samples with high TGFβ signaling and TEM gene signature activation score classified as “high TEM/TGFβ signature” versus the remainder (“low TEM/TGFβ signature”). (F) Representative breast cancer section (from n=20) stained with CD14 (red) and podoplanin (brown). Scale bar, 100 µm. Zoomed inset demonstrates CD14+ macrophages associated with podoplanin+ lymphatic vasculature (black arrows). Tissues selected from 8 patients with/without lymph node

positivity. Consecutive sections were stained singly for podoplanin lymphovasculature, or doubly using pan-macrophage marker, CD68 and anti-b4 integrin antibody. (G) Double stained macrophages per mm^2 shown with patient clinical details (LVI and lymph node positivity). CD68+ITGB4+ macrophages indicated in upper right panels (red arrows) and CD68 and ITGB4 staining shown below as 2 single panels, CD68+ITGB4+ macrophages indicated with red arrow. Podoplanin+ vessels shown in upper left images (black arrows). Scale bar, 20 µm.

STAR METHODS

Contact for reagent and Resource Sharing

Further information and requests for resources and reagents should be directed to the Lead Contact, Tony Ng (tony.ng@kcl.ac.uk)

For a detailed description of the experimental procedures please see supplementary information.

Experimental Model and Subject Details

Tissue culture

Bone marrow macrophages: Monocytes were isolated from female BALB/c mice femurs and cultured in mCSF-1 for 5 d.

Cell lines: All cell lines were tested as mycoplasma negative and authenticated by IDEXX Laboratories Ltd, UK.

Tumor-bearing mice

4T1.2 : BALB/c immune-competent mice were 6–8 weeks of age and maintained under pathogen-free conditions. Tumors were established by injection of $1x10^6$ 4T1.2 cells into the mammary fat pad.

BLG-Cre;Brca1$^{f/f}$,p53$^{+/-}$: Mammary tumor chunks (approximately $0.2cm^3$) dissected from BLG-Cre;Brca1$^{f/f}$,p53$^{+/-}$ mice (Molyneux et al., 2010) were transplanted orthotopically into mammary fat pads of recipient 5-week old C57BL6J mice. Tumors were grown for 4-8 weeks before mice were culled and tumor tissues harvested.

Human breast cancer samples

Paraffin embedded samples (n=20) (KHP Cancer Biobank Molecular Taxonomy of Breast Cancer International Consortium (METABRIC) dataset cohort) were used. Ten patients were previously characterized as having lymphatic vessel invasion (LVI) and the remaining 10 did not have LVI. Please see SI for details on staining.

Study approval

All experiments were performed in accordance with the local ethical review panel, the UK Home Office Animals Scientific Procedures Act, 1986 and the UKCCCR guidelines.

Method Details

RAW264.7 macrophage treatment

Tumor-bearing mice were injected with 100 μl PBS or $1x10^6$ RAW264.7 macrophages starting on the second day after tumor inoculation and repeated every 2 days until the end of the experiment.

Clodronate treatment

Endogenous macrophages were ablated using clodronate-containing liposomes (Weisser et al., 2012).

Immunofluorescence

Tissue sections were fixed with 4% paraformaldehyde (PFA), blocked in 5% BSA followed by staining. Hoechst-33342 (0.1 µg/ml) was used for nuclear staining and samples mounted using Mowiol (with DABCO). Image acquisition by confocal microscopy was performed using a Nikon Eclipse Ni-E Upright. Image acquisition was conducted using NIS Elements C software and analyzed using Image J software.

Image acquisition and analysis for colocalization studies in tissue

Cy3 and AF647 dyes were imaged before and after photobleaching using (x20 0.75NA air objective, Nikon) and a cooled CCD detector (Hamamatsu ORCA-03G, 1024 x 1024) with respective integration time of 100 ms and 1000 ms. Dyes were photobleached using a mode-locked Titanium Sapphire Laser (Coherent, Chameleon Ultra 2) tuned at 730 nm with pulse duration of about 200 fs, a repetition rate of 80 MHz and average laser power on the sample of 30 mW. To measure the relative level of β4 integrin expression within the lymphovasculature compared with the rest of the tissue, we measured average AF647 intensity within lymphovasculature areas (high Cy3 intensity) normalized by the average AF647 intensity outside lymphovasculature areas (low Cy3 intensity).

Structured Illumination Microscopy (SIM)

RAW264.7-NTC or RAW264.7-TGFβ1 KD were stained with rat anti-β4 integrin antibody and anti-rat AF647 antibody. Image acquisition by SIM was performed using Nikon N-SIM microscope equipped with a 640nm laser, a Andor iXon Ultra 897 EMCCD camera and a 100x 1.49NA oil immersion objective. Images were analyzed using ImageJ software.

Mammary imaging window implantation and intravital microscopy

Mammary Imaging Window (MIW) surgery was performed 10-14 days after tumor innoculation (Kedrin et al., 2008). Images shown are representative of a minimum of

5 independent experiments.For imaging lymphatic vasculature, mice were injected subcutaneously at the tail base with 50 μl 76kDa dextran-fluorescein or dextran-Texas red 15 min prior to imaging. Mice were imaged for a maximum period of 4 h per day using a x20 air objective. All post-hoc image processing and image reconstructions were done using Image J software.

Lymphatic vessel permeability

Tumor-bearing mice were injected subcutaneously at the tail base with 1% Evans Blue dye. After 30 min the mice were culled and the tumors incubated in formamide overnight at 55°C. Optical density of formamide was read at 620nm and quantification of lymphatic permeability was given as OD per g tumor.

Adhesion assay

Laminin-5 was plated onto 96 well plates overnight at 4°C and non-specific interactions blocked with BSA. Macrophages (5×10^{6}/ml) were labeled with 1 μM 2′,7′-bis-(2-carboxyethyl)-5-(and-6)-carboxyfluorescein-acetoxymethyl ester (BCECF) for 30 min at room temperature. 100μl of cells (1×10^{6}/ml) were added at 37°C, plates washed, and adhering macrophages quantified using a fluorescence microtiter plate reader.

Lymphatic endothelial cell contraction

SV-LEC cells or primary lymphatic endothelial cells were grown as a monolayer. On day 3 LECs and macrophages were stained for 30min at 37°C using 1μg/ml CMTMR or CMFDA respectively. Macrophages were added to SV-LEC monolayers overnight. Confocal images of the co-culture and the area around individual SV-LECs was calculated using ImageJ software.

RhoA biosensor

SV-LECs were transiently transfected with the Raichu RhoA biosensor (Yoshizaki et al., 2003). The biosensor was modified to express GFP and mRFP (Makrogianneli et al., 2009). Multiphoton time-correlated single photon counting FLIM was performed to quantify RhoA biosensor FRET Fluorescence excitation was provided by a Fianium laser, which generates optical pulses with a duration of 40 ps at a repetition rate of 80 MHz. For the imaging of Raichu-transfected SV-LECs, multi-photon excitation was employed using a solid-state pumped (8-W Verdi; Coherent), femtosecond self-mode locked Ti:Sapphire (Mira; Coherent) laser system (Peter et al., 2005, Barber et al.,

2009). Imaging data comprised of 256 x 256 pixel resolution and 256 time channels. The fluorescence lifetime was calculated as described (Barber et al., 2013).

TGFβ1 stable knockdown in RAW264.7 macrophages

Stable TGFβ1 knockdown RAW 264.7 macrophage lines were generated by lentiviral transduction using the pGIPZ system (Open Biosystems). Viral packaging was performed by transiently transfecting HEK293T cells with the pGIPZ shRNA transfer vector and the accessory plasmids pCMV-dR8.91 and pMD2G. Stable cell lines were established using three different shRNA lentiviral vectors. RAW 264.7 macrophages were cultured in puromycin (1 µg/ml) to enable the selection of successfully transduced cells and efficacy of knockdown was assessed by western blotting.

FACS analysis

RAW264.7 cell lines (TGFβ1-knockdown or NTC) were stained with a Live-Dead Yellow dye followed by staining with a primary rat anti-β4 integrin antibody and anti-rat AF647-conjugated secondary antibody.

Tumors were disaggregated with Collagenase (Sigma UK) and DNase I (Applichem, UK) before staining with Live-Dead Yellow, CD45-APC Cy7, Ly6G-Biotin + Streptavidin AF488, CD11b-eFluor450, Tie-2 PE β4 integrin-BV711 and CD31 PerCPCy5.5. Cells were fixed with 1% PFA and analysed in a FACS Canto II (BD Biosciences) cytometer. Data analysed using FlowJo software (TreeStar Inc., Ashland, OR, USA).

Human tissue staining

Sections were stained using anti-CD14/anti-podoplanin using Ventana Benchmark Ultra and Ultra view DAB and Alkaline Phosphatase detection systems. Sections were assessed independently by two histopathologists and scored for CD14+ macrophages within or proximal to lymphatic vasculature.

Alternatively, using consecutive sections the first section was stained with anti-podoplanin and the second section stained with anti-ITGB4 anti-CD68. All sections were stained with DAB+ substrate/chromagen. All incubations were at room temperature.

The slides were scanned in the Hamamatsu NanoZoomer S210 Digital slide scanner. The image analysis was performed on the whole section with the color deconvolution module and the positive pixel algorithm from QuPath image analysis software.

Quantification and Statistical Analysis

Gene expression microarray analysis

RNA was extracted from macrophage cell cultures and profiled using Affymetrix Mouse Gene 1.0 ST arrays. Differential expression between conditions was estimated by fitting a linear model and performing empirical Bayes moderated *t*-tests using the package 'limma' (v3.22.4) (Ritchie et al., 2015). The expression score for a specific gene in each sample is defined as the weighted sum of gene-standardized (*Z*-score) expression values, with weights +1/-1 according to relative increase or decrease in BMM + 4T1.2 compared with BMM.

Analysis of gene signatures

To establish ITGB4 expression and assess association between ITGB4 expression and activation of the TGFβ signaling in macrophages, processed gene counts were obtained from the ARCHS4 database (Lachmann et al., 2018) and further normalized for downstream analyses. Enrichment of TGFβ signaling was computed using the ssGSEA method (Barbie et al., 2009) as implemented in the GSVA package from Bioconductor.

False zero expression due to dropout events in scRNA-seq data was corrected using the scImpute algorithm as previously described (Li and Li, 2018). scRNAseq data is reported as log2(TPM+1).

Macrophage-mediated vascular remodeling pathway signature (Pucci et al., 2009) was converted to a human gene list using Biomart ID conversion (Ensembl Genes 84// mus musculus genes GRCm38.p4). TGFβ (KEGG) gene signature was derived from (MSigDB). Gene signature activity was calculated using a weighted average sum over all genes for each tumor. Pearson's correlation between the activation scores was reported. Hypergeometric testing was used to establish the significance of overlap between TNBC with distant metastasis (DM) on those of dual high activation scores. Kaplan-Meier plots were generated for each data set to provide a visualization of survival stratification.

All other statistical analysis is described in the text and legends and was preformed using Prism software (GraphPad). P values less than 0.05 were considered significant. The statistical test used is indicated in the figure legends and the significance of findings is indicated in the figures.

Data and software availability: Experiment ArrayExpress accession: E-MTAB-4064.

ANDO, T., JORDAN, P., JOH, T., WANG, Y., JENNINGS, M. H., HOUGHTON, J. & ALEXANDER, J. S. 2005. Isolation and characterization of a novel mouse lymphatic endothelial cell line: SV-LEC. *Lymphat Res Biol,* 3**,** 105-15.

AVRAAMIDES, C. J., GARMY-SUSINI, B. & VARNER, J. A. 2008. Integrins in angiogenesis and lymphangiogenesis. *Nat Rev Cancer,* 8**,** 604-17.

BALKWILL, F. R., CAPASSO, M. & HAGEMANN, T. 2012. The tumor microenvironment at a glance. *J Cell Sci,* 125**,** 5591-6.

BARBER, P. R., AMEER-BEG, S. M., GILBEY, J., CARLIN, L. M., KEPPLER, M., NG, T. C. & VOJNOVIC, B. 2009. Multiphoton time-domain fluorescence lifetime imaging microscopy: practical application to protein-protein interactions using global analysis. *Journal of the Royal Society Interface,* 6**,** S93-S105.

BARBER, P. R., TULLIS, I. D., PIERCE, G. P., NEWMAN, R. G., PRENTICE, J., ROWLEY, M. I., MATTHEWS, D. R., AMEER-BEG, S. M. & VOJNOVIC, B. 2013. The Gray Institute 'open' high-content, fluorescence lifetime microscopes. *J Microsc,* 251**,** 154-67.

BARBIE, D. A., TAMAYO, P., BOEHM, J. S., KIM, S. Y., MOODY, S. E., DUNN, I. F., SCHINZEL, A. C., SANDY, P., MEYLAN, E., SCHOLL, C., FROHLING, S., CHAN, E. M., SOS, M. L., MICHEL, K., MERMEL, C., SILVER, S. J., WEIR, B. A., REILING, J. H., SHENG, Q., GUPTA, P. B., WADLOW, R. C., LE, H., HOERSCH, S., WITTNER, B. S., RAMASWAMY, S., LIVINGSTON, D. M., SABATINI, D. M., MEYERSON, M., THOMAS, R. K., LANDER, E. S., MESIROV, J. P., ROOT, D. E., GILLILAND, D. G., JACKS, T. & HAHN, W. C. 2009. Systematic RNA interference reveals that oncogenic KRAS-driven cancers require TBK1. *Nature,* 462**,** 108-12.

BRON, S., HENRY, L., FAES-VAN'T HULL, E., TURRINI, R., VANHECKE, D., GUEX, N., IFTICENE-TREBOUX, A., MARINA IANCU, E., SEMILIETOF, A., RUFER, N., LEHR, H. A., XENARIOS, I., COUKOS, G., DELALOYE, J. F. & DOUCEY, M. A. 2016. TIE-2-expressing monocytes are lymphangiogenic and associate specifically with lymphatics of human breast cancer. *Oncoimmunology,* 5**,** e1073882.

BRYAN, B. A., DENNSTEDT, E., MITCHELL, D. C., WALSHE, T. E., NOMA, K., LOUREIRO, R., SAINT-GENIEZ, M., CAMPAIGNIAC, J. P., LIAO, J. K. & D'AMORE, P. A. 2010. RhoA/ROCK signaling is essential for multiple aspects of VEGF-mediated angiogenesis. *FASEB J,* 24**,** 3186-95.

CARLIN, L. M., EVANS, R., MILEWICZ, H., FERNANDES, L., MATTHEWS, D. R., PERANI, M., LEVITT, J., KEPPLER, M. D., MONYPENNY, J., COOLEN, T., BARBER, P. R., VOJNOVIC, B., SUHLING, K., FRATERNALI, F., AMEER-BEG, S., PARKER, P. J., THOMAS, N. S. & NG, T. 2011. A targeted siRNA screen identifies regulators of Cdc42 activity at the natural killer cell immunological synapse. *Sci Signal,* 4**,** ra81.

CHOI, W. W., LEWIS, M. M., LAWSON, D., YIN-GOEN, Q., BIRDSONG, G. G., COTSONIS, G. A., COHEN, C. & YOUNG, A. N. 2005. Angiogenic and lymphangiogenic microvessel density in breast carcinoma: correlation with clinicopathologic parameters and VEGF-family gene expression. *Mod Pathol,* 18**,** 143-52.

CONDEELIS, J. & POLLARD, J. W. 2006. Macrophages: obligate partners for tumor cell migration, invasion, and metastasis. *Cell,* 124**,** 263-6.

DE PALMA, M., MURDOCH, C., VENNERI, M. A., NALDINI, L. & LEWIS, C. E. 2007. Tie2-expressing monocytes: regulation of tumor angiogenesis and therapeutic implications. *Trends Immunol,* 28**,** 519-24.

DE PALMA, M., VENNERI, M. A., GALLI, R., SERGI SERGI, L., POLITI, L. S., SAMPAOLESI, M. & NALDINI, L. 2005. Tie2 identifies a hematopoietic lineage of proangiogenic monocytes required for tumor vessel formation and a mesenchymal population of pericyte progenitors. *Cancer Cell,* 8**,** 211-26.

DENT, R., TRUDEAU, M., PRITCHARD, K. I., HANNA, W. M., KAHN, H. K., SAWKA, C. A., LICKLEY, L. A., RAWLINSON, E., SUN, P. & NAROD, S. A. 2007. Triple-negative breast cancer: clinical features and patterns of recurrence. *Clin Cancer Res,* 13**,** 4429-34.

DESGROSELLIER, J. S. & CHERESH, D. A. 2010. Integrins in cancer: biological implications and therapeutic opportunities. *Nat Rev Cancer,* 10**,** 9-22.

DIAZ, L. K., CRISTOFANILLI, M., ZHOU, X., WELCH, K. L., SMITH, T. L., YANG, Y., SNEIGE, N., SAHIN, A. A. & GILCREASE, M. Z. 2005. Beta4 integrin subunit gene expression correlates with tumor size and nuclear grade in early breast cancer. *Mod Pathol,* 18**,** 1165-75.

EVANS, R., PATZAK, I., SVENSSON, L., DE FILIPPO, K., JONES, K., MCDOWALL, A. & HOGG, N. 2009. Integrins in immunity. *J Cell Sci,* 122**,** 215-25.

FINSTERBUSCH, M., VOISIN, M. B., BEYRAU, M., WILLIAMS, T. J. & NOURSHARGH, S. 2014. Neutrophils recruited by chemoattractants in vivo induce microvascular plasma protein leakage through secretion of TNF. *J Exp Med,* 211**,** 1307-14.

FLEMING, Y. M., FERGUSON, G. J., SPENDER, L. C., LARSSON, J., KARLSSON, S., OZANNE, B. W., GROSSE, R. & INMAN, G. J. 2009. TGF-beta-mediated activation of RhoA signalling is required for efficient (V12)HaRas and (V600E)BRAF transformation. *Oncogene,* 28**,** 983-93.

GAZINSKA, P., GRIGORIADIS, A., BROWN, J. P., MILLIS, R. R., MERA, A., GILLETT, C. E., HOLMBERG, L. H., TUTT, A. N. & PINDER, S. E. 2013. Comparison of basal-like triple-negative breast cancer defined by morphology, immunohistochemistry and transcriptional profiles. *Mod Pathol,* 26**,** 955-66.

GORDON, E. J., RAO, S., POLLARD, J. W., NUTT, S. L., LANG, R. A. & HARVEY, N. L. 2010. Macrophages define dermal lymphatic vessel calibre during development by regulating lymphatic endothelial cell proliferation. *Development,* 137**,** 3899-910.

HARNEY, A. S., ARWERT, E. N., ENTENBERG, D., WANG, Y., GUO, P., QIAN, B. Z., OKTAY, M. H., POLLARD, J. W., JONES, J. G. & CONDEELIS, J. S. 2015. Real-Time Imaging Reveals Local, Transient Vascular Permeability, and Tumor Cell Intravasation Stimulated by TIE2hi Macrophage-Derived VEGFA. *Cancer Discov,* 5**,** 932-43.

HEASMAN, S. J., CARLIN, L. M., COX, S., NG, T. & RIDLEY, A. J. 2010. Coordinated RhoA signaling at the leading edge and uropod is required for T cell transendothelial migration. *J Cell Biol,* 190**,** 553-63.

HYNES, R. O. 2002. Integrins: bidirectional, allosteric signaling machines. *Cell,* 110**,** 673-87.

INMAN, G. J., NICOLAS, F. J., CALLAHAN, J. F., HARLING, J. D., GASTER, L. M., REITH, A. D., LAPING, N. J. & HILL, C. S. 2002. SB-431542 is a potent and specific inhibitor of transforming growth factor-beta superfamily type I activin receptor-like kinase (ALK) receptors ALK4, ALK5, and ALK7. *Mol Pharmacol,* 62**,** 65-74.

KEDRIN, D., GLIGORIJEVIC, B., WYCKOFF, J., VERKHUSHA, V. V., CONDEELIS, J., SEGALL, J. E. & VAN RHEENEN, J. 2008. Intravital imaging of metastatic behavior through a mammary imaging window. *Nat Methods,* 5**,** 1019-21.

KITAMURA, T., QIAN, B. Z., SOONG, D., CASSETTA, L., NOY, R., SUGANO, G., KATO, Y., LI, J. & POLLARD, J. W. 2015. CCL2-induced chemokine cascade promotes breast cancer metastasis by enhancing retention of metastasis-associated macrophages. *J Exp Med,* 212**,** 1043-59.

LACHMANN, A., TORRE, D., KEENAN, A. B., JAGODNIK, K. M., LEE, H. J., WANG, L., SILVERSTEIN, M. C. & MA'AYAN, A. 2018. Massive mining of publicly available RNA-seq data from human and mouse. *Nat Commun,* 9**,** 1366.

LI, W. V. & LI, J. J. 2018. An accurate and robust imputation method scImpute for single-cell RNA-seq data. *Nat Commun,* 9**,** 997.

LIU, H. T., MA, R., YANG, Q. F., DU, G. & ZHANG, C. J. 2009. Lymphangiogenic characteristics of triple negativity in node-negative breast cancer. *Int J Surg Pathol,* 17**,** 426-31.

LU, S., SIMIN, K., KHAN, A. & MERCURIO, A. M. 2008. Analysis of integrin beta4 expression in human breast cancer: association with basal-like tumors and prognostic significance. *Clin Cancer Res,* 14**,** 1050-8.

MAKROGIANNELI, K., CARLIN, L. M., KEPPLER, M. D., MATTHEWS, D. R., OFO, E., COOLEN, A., AMEER-BEG, S. M., BARBER, P. R., VOJNOVIC, B. & NG, T. 2009. Integrating receptor signal inputs that influence small Rho GTPase activation dynamics at the immunological synapse. *Mol Cell Biol,* 29**,** 2997-3006.

MELCHOR, L., MOLYNEUX, G., MACKAY, A., MAGNAY, F. A., ATIENZA, M., KENDRICK, H., NAVA-RODRIGUES, D., LOPEZ-GARCIA, M. A., MILANEZI, F., GREENOW, K., ROBERTSON, D., PALACIOS, J., REIS-FILHO, J. S. & SMALLEY, M. J. 2014. Identification of cellular and genetic drivers of breast cancer heterogeneity in genetically engineered mouse tumour models. *J Pathol,* 233**,** 124-37.

MOHAMMED, R. A., ELLIS, I. O., MAHMMOD, A. M., HAWKES, E. C., GREEN, A. R., RAKHA, E. A. & MARTIN, S. G. 2011. Lymphatic and blood vessels in basal and triple-negative breast cancers: characteristics and prognostic significance. *Mod Pathol,* 24**,** 774-85.

MOHAMMED, R. A., MARTIN, S. G., GILL, M. S., GREEN, A. R., PAISH, E. C. & ELLIS, I. O. 2007. Improved methods of detection of lymphovascular invasion demonstrate that it is the predominant method of vascular invasion in breast cancer and has important clinical consequences. *Am J Surg Pathol,* 31**,** 1825-33.

MOLYNEUX, G., GEYER, F. C., MAGNAY, F. A., MCCARTHY, A., KENDRICK, H., NATRAJAN, R., MACKAY, A., GRIGORIADIS, A., TUTT, A., ASHWORTH, A., REIS-FILHO, J. S. & SMALLEY, M. J. 2010. BRCA1 basal-like breast cancers originate from luminal epithelial progenitors and not from basal stem cells. *Cell Stem Cell,* 7**,** 403-17.

PETER, M., AMEER-BEG, S. M., HUGHES, M. K., KEPPLER, M. D., PRAG, S., MARSH, M., VOJNOVIC, B. & NG, T. 2005. Multiphoton-FLIM quantification of the EGFP-mRFP1 FRET pair for localization of membrane receptor-kinase interactions. *Biophys J,* 88**,** 1224-37.

POLLARD, J. W. 2004. Tumour-educated macrophages promote tumour progression and metastasis. *Nat Rev Cancer,* 4**,** 71-8.

PUCCI, F., VENNERI, M. A., BIZIATO, D., NONIS, A., MOI, D., SICA, A., DI SERIO, C., NALDINI, L. & DE PALMA, M. 2009. A distinguishing gene signature shared by tumor-infiltrating Tie2-expressing monocytes, blood "resident" monocytes, and embryonic macrophages suggests common functions and developmental relationships. *Blood,* 114**,** 901-14.

QUAIL, D. F. & JOYCE, J. A. 2013. Microenvironmental regulation of tumor progression and metastasis. *Nat Med,* 19**,** 1423-37.

RAMSAY, A. G., EVANS, R., KIAII, S., SVENSSON, L., HOGG, N. & GRIBBEN, J. G. 2013. Chronic lymphocytic leukemia cells induce defective LFA-1-directed T-cell motility by altering Rho GTPase signaling that is reversible with lenalidomide. *Blood,* 121**,** 2704-14.

RITCHIE, M. E., PHIPSON, B., WU, D., HU, Y., LAW, C. W., SHI, W. & SMYTH, G. K. 2015. limma powers differential expression analyses for RNA-sequencing and microarray studies. *Nucleic Acids Res,* 43**,** e47.

SAVAGE, N. D., DE BOER, T., WALBURG, K. V., JOOSTEN, S. A., VAN MEIJGAARDEN, K., GELUK, A. & OTTENHOFF, T. H. 2008. Human anti-inflammatory macrophages induce Foxp3+ GITR+ CD25+ regulatory T cells, which suppress via membrane-bound TGFbeta-1. *J Immunol,* 181**,** 2220-6.

STEWART, R. L. & O'CONNOR, K. L. 2015. Clinical significance of the integrin alpha6beta4 in human malignancies. *Lab Invest,* 95**,** 976-86.

VEGA, F. M., FRUHWIRTH, G., NG, T. & RIDLEY, A. J. 2011. RhoA and RhoC have distinct roles in migration and invasion by acting through different targets. *J Cell Biol,* 193**,** 655-65.

WANG, S. E., XIANG, B., ZENT, R., QUARANTA, V., POZZI, A. & ARTEAGA, C. L. 2009. Transforming growth factor beta induces clustering of HER2 and integrins by activating Src-focal adhesion kinase and receptor association to the cytoskeleton. *Cancer Res,* 69**,** 475-82.

WEISSER, S. B., VAN ROOIJEN, N. & SLY, L. M. 2012. Depletion and reconstitution of macrophages in mice. *J Vis Exp***,** 4105.

WONG, S. Y. & HYNES, R. O. 2006. Lymphatic or hematogenous dissemination: how does a metastatic tumor cell decide? *Cell Cycle,* 5**,** 812-7.

YOSHIZAKI, H., OHBA, Y., KUROKAWA, K., ITOH, R. E., NAKAMURA, T., MOCHIZUKI, N., NAGASHIMA, K. & MATSUDA, M. 2003. Activity of Rho-family GTPases during cell division as visualized with FRET-based probes. *J Cell Biol,* 162**,** 223-32.

KEY RESOURCES TABLE

REAGENT or RESOURCE	SOURCE	IDENTIFIER
Antibodies		
Rat monoclonal anti-Lyve1	Novus Biologicals	#NB-600-1008
Rabbit polyclonal anti-Tie2 (C-20)	Santa Cruz	#sc-324
Rabbit polyclonal phospho-Smad2/3 (D27F4)	Cell Signaling	#8828
Mouse monoclonal anti-ITGB4	Abcam	#ab29042
Mouse monoclonal anti-CD68 antibody	Ventana Cell Marque	#168M
Mouse monoclonal anti-CD14 (EPR3653)	Ventana Cell Marque	#114R
Mouse monoclonal anti-podoplanin (D2-40)	Ventana Cell Marque	#332M
Rat monoclonal anti-CD45-APC-Cy7	Biolegend	#103115
Rat monoclonal Ly6G-Biotin	Biolegend	#127603
Streptavidin AF488	Biolegend	#405235
Rat monoclonal CD11b-eFluor450	ThermoFisher Scientific	#48-0112-82
Rat monoclonal Tie-2 PE	Biolegend	#124007
Rat monoclonal β4 integrin-BV711	BDBiosciences	#744154
CD31 PerCPCy5.5	Biolegend	#102419
Rat monoclonal anti-F4/80-FITC (clone BM8)	Abcam	#Ab60348
Rabbit polyclonal anti-laminin-5	Abcam	#Ab14509
Rabbit polycloncal Anti-Phospho myson light chain (Ser19)	Cell Signaling	#3671
Mouse monoclonal anti-podoplanin antibody	Santa Cruz	#sc-166906
Rabbit polyclonal anti-TGFb1 antibody	Proteintech	#11522-1-AP
Biological Samples		

Breast cancer tumor tissues (paraffin-embedded)	King's College London breast cancer biobank	Team lead – Dr Cheryl Gillet
4T1.2 tumor tissues (frozen)	King's College London	Dr Rachel Evans
BLG-Cre;Brca1$^{f/f}$,p53$^{+/-}$ tumor tissues (frozen)	King's College London	Dr Rebecca Marlow
Chemicals, Peptides, and Recombinant Proteins		
Cell tracker™ red (CMTMR) and Cell tracker™ green (CMFDA)	Life Technologies	#C34552, C2925
Murine CSF1	Sigma	#M9170
Human recombinant laminin-5	Novus Biologicals	#H00003911
Clodronate and PBS liposomes	Liposoma Technology	#CP-005-005
2′,7′-bis-(2-carboxyethyl)-5-(and-6)-carboxyfluorescein-acetoxymethyl ester (BCECF)	Thermo Scientific	#B1170
SB-431542	Sigma	#S4317
Evans Blue dye	Sigma	#E2129
Formamide	Sigma	#F9037
76kDa dextran Texas Red	Sigma	#R05027
76kDa dextran fluorescein	Santa Cruz	#sc-263323
Critical Commercial Assays		
Murine TGFb1 quantikine ELISA kit	R&D Ltd	#MB100B
Murine TGFb2 quantikine ELISA kit	R&D Ltd	#DB250
Deposited Data		
Experiment ArrayExpress accession	Array Express	#E-MTAB-4064.
Breast Cancer Gene Expression data	Gene Expression Omnibus	#GSE75688

ARCHS4 database	(Lachmann et al., 2018)	N/A
Experimental Models: Cell Lines		
4T1.2 cells derived from female BALB/C mouse	(Lelekakis et al., 1999)	N/A
SV-LEC (derived from male “immortomouse”)	(Ando et al., 2005)	Gift from Dr Steven Alexander
Primary LEC from male BALB/C mouse	Generon Ltd	#BALB5064L
RAW264.7 derived from male BALB/C mouse	ATCC Ltd	#ATCC-TIB71
HEK293T (derived from human fetus)	ATCC Ltd	#ATCC-CRL-11268
Experimental Models: Organisms/Strains		
Female BALB/c mice	Charles River	N/A
Female C57Bl6J mice	Charles River	N/A
Oligonucleotides		
Raichu RhoA biosensor construct	King’s College London	(Heasman et al., 2010)
GFP-RhoA construct	King’s College London	(Heasman et al., 2010)
Software and Algorithms		
TRI2 https://app.assembla.com/spaces/ATD_TRI/wiki	Gray Laboratories Oxford University and University College London	Dr Paul Barber (Barber et al., 2013)
Prism Software	https://www.graphpad.com/scientific-software/prism/	N/A

ImageJ (Fiji)	https://imagej.nih.gov/ij/	N/A
Colocalisation plugin for ImageJ	(within this manuscript)	Dr Fred Festy
Other		
TGFb1 shRNA (GIPZ)	Open Biosystems	University College London library
ITGB4 shRNA (GIPZ)	Open Biosystems	University College London
RNA easy minikit	Quiagen	#74104
Live/Dead Yellow dye	Invitrogen	#L34959
Affymetrix Mouse Gene 1.0 ST arrays	Thermo Scientific	#901168

Figure 1

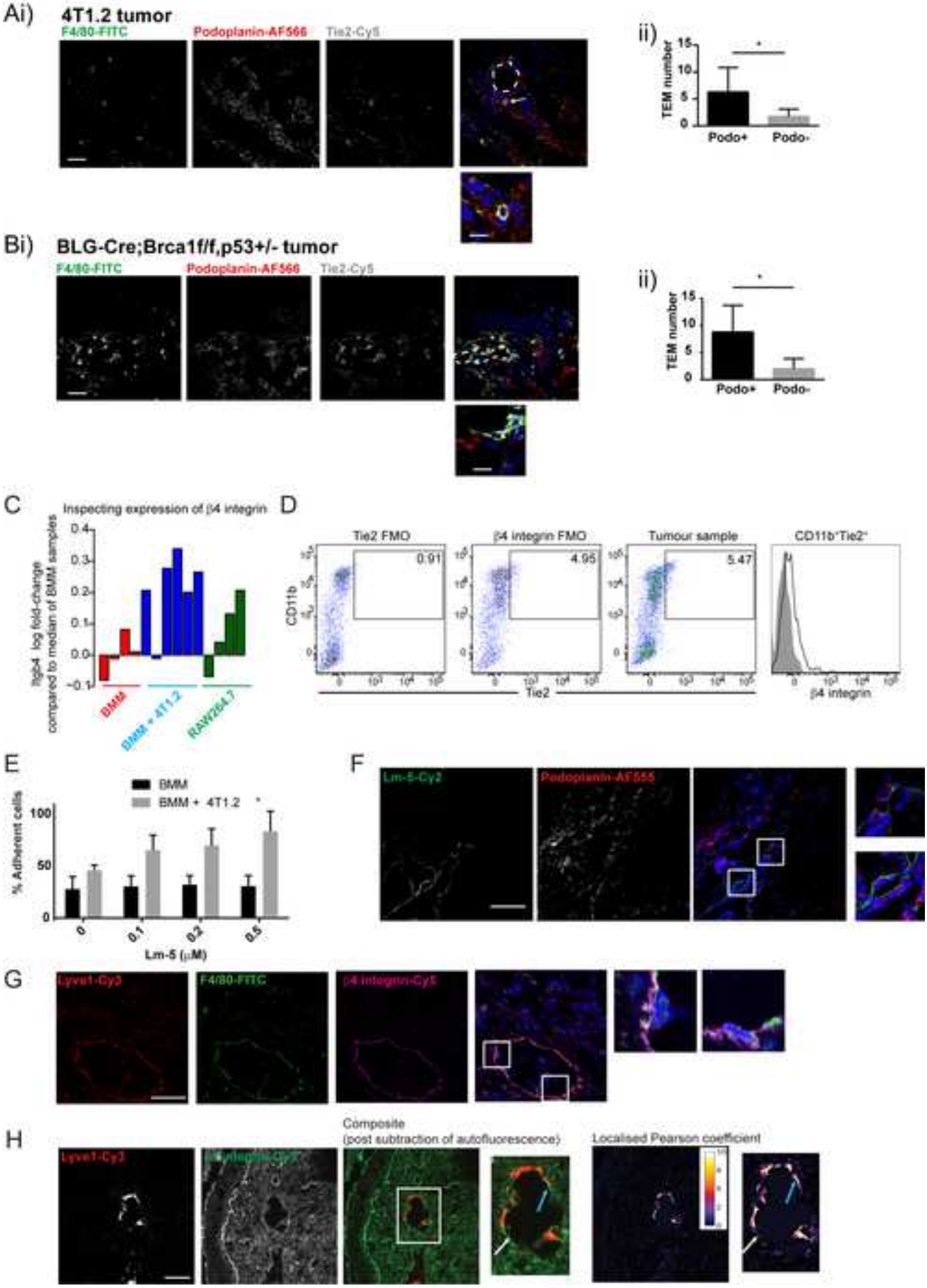
Ai)
4T1.2 tumor
F4/80-FITC
Podoplanin-AF566
Tie2-Cy5
ii)
TEM number
Podo+
Podo-
Bi)
BLG-Cre;Brca1f/f,p53+/- tumor
F4/80-FITC
Podoplanin-AF566
Tie2-Cy5
ii)
TEM number
Podo+
Podo-
C
Inspecting expression of β4 integrin
Itgb4 log fold-change compared to median of BMM samples
BMM
BMM + 4T1.2
RAW264.7
D
Tie2 FMO
β4 integrin FMO
Tumour sample
CD11b+Tie2+
CD11b
Tie2
β4 integrin
E
BMM
BMM + 4T1.2
% Adherent cells
Lm-5 (μM)
F
Lm-5-Cy2
Podoplanin-AF555
G
Lyve1-Cy3
F4/80-FITC
β4 integrin-Cy5
H
Lyve1-Cy3
Composite
(post subtraction of autofluorescence)
Localised Pearson coefficient

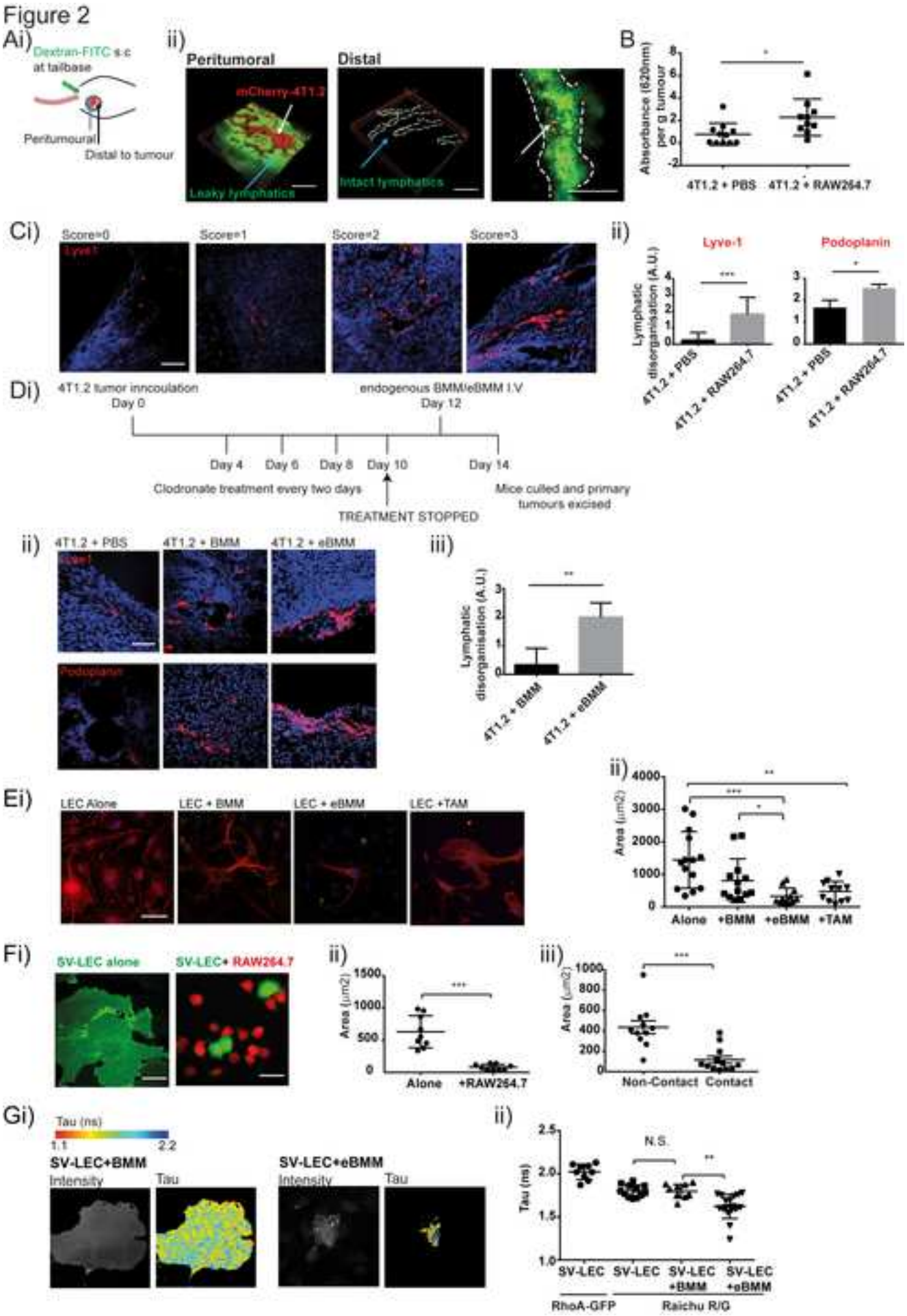
Figure 2
Ai)
Dextran-FITC s.c at tailbase
Peritumoural
Distal to tumour
ii)
Peritumoral
Distal
mCherry-4T1.2
Leaky lymphatics
Intact lymphatics
B
Absorbance (620nm) per g tumour
4T1.2 + PBS
4T1.2 + RAW264.7
Ci)
Score=0
Score=1
Score=2
Score=3
Lyve-1
ii)
Lymphatic disorganisation (A.U.)
Podoplanin
Di)
4T1.2 tumor inncoulation Day 0
endogenous BMM/eBMM I.V Day 12
Day 4
Day 6
Day 8
Day 10
Day 14
Clodronate treatment every two days
TREATMENT STOPPED
Mice culled and primary tumours excised
ii)
4T1.2 + PBS
4T1.2 + BMM
4T1.2 + eBMM
iii)
Lymphatic disorganisation (A.U.)
Ei)
LEC Alone
LEC + BMM
LEC + eBMM
LEC +TAM
ii)
Area (µm2)
Alone
+BMM
+eBMM
+TAM
Fi)
SV-LEC alone
SV-LEC+ RAW264.7
ii)
Area (µm2)
Alone
+RAW264.7
iii)
Area (µm2)
Non-Contact
Contact
Gi)
Tau (ns)
1.1
2.2
SV-LEC+BMM
Intensity
Tau
SV-LEC+eBMM
Intensity
Tau
ii)
Tau (ns)
N.S.
SV-LEC
SV-LEC
SV-LEC +BMM
SV-LEC +eBMM
RhoA-GFP
Raichu R/G

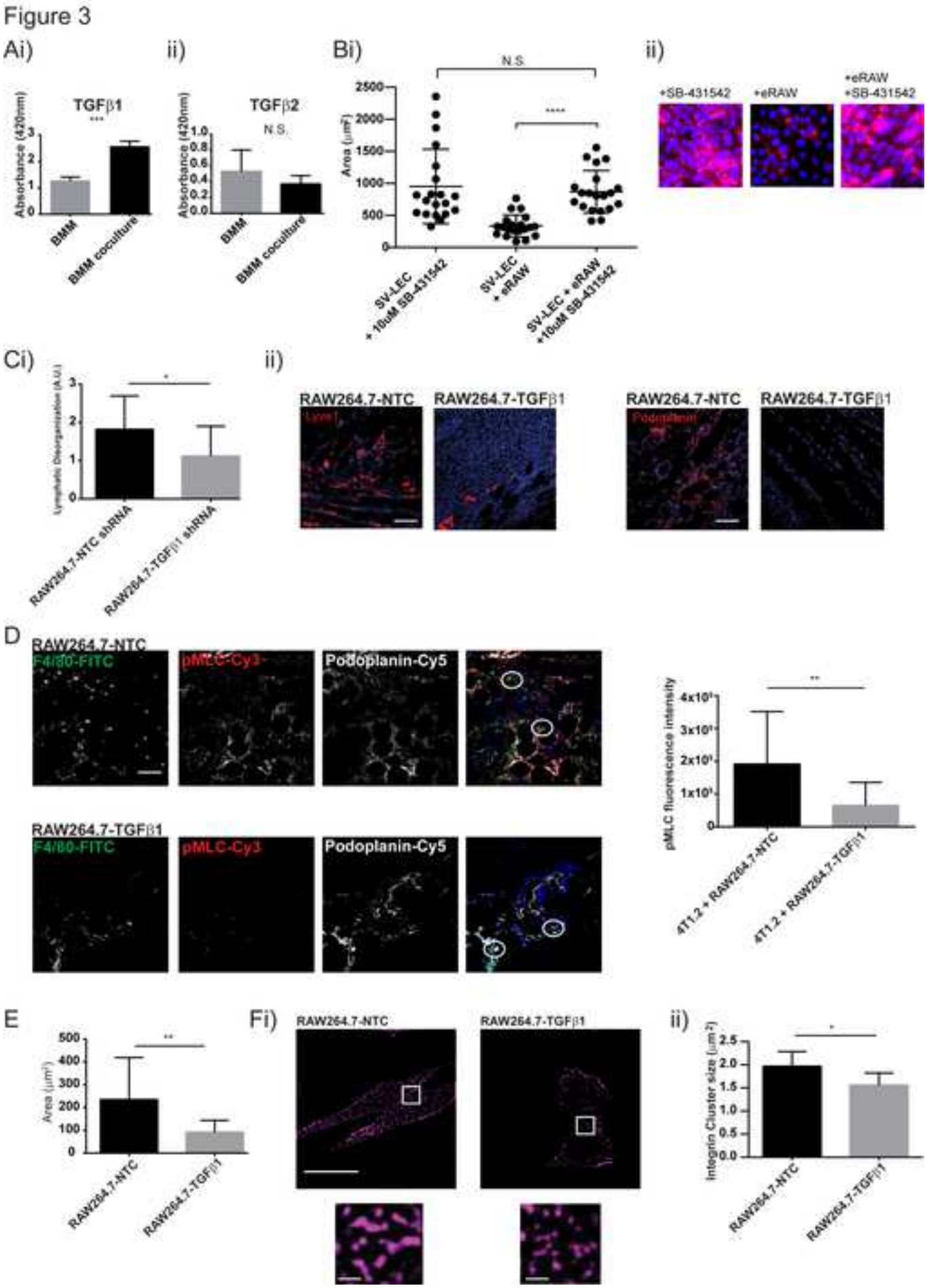
Figure 3
Ai)
ii)
TGFβ1
TGFβ2
N.S.
Absorbance (420nm)
BMM
BMM coculture
Bi)
N.S.
****
Area (μm²)
SV-LEC + 10uM SB-431542
SV-LEC + eRAW
SV-LEC + eRAW +10uM SB-431542
ii)
+SB-431542
+eRAW
+eRAW +SB-431542
Ci)
Lymphatic Disorganization (A.U.)
RAW264.7-NTC shRNA
RAW264.7-TGFβ1 shRNA
ii)
RAW264.7-NTC
RAW264.7-TGFβ1
Podoplanin
D
RAW264.7-NTC
F4/80-FITC
pMLC-Cy3
Podoplanin-Cy5
RAW264.7-TGFβ1
pMLC fluorescence intensity
4T1.2 + RAW264.7-NTC
4T1.2 + RAW264.7-TGFβ1
E
Area (μm²)
RAW264.7-NTC
RAW264.7-TGFβ1
Fi)
ii)
Integrin Cluster size (μm²)

Figure 4

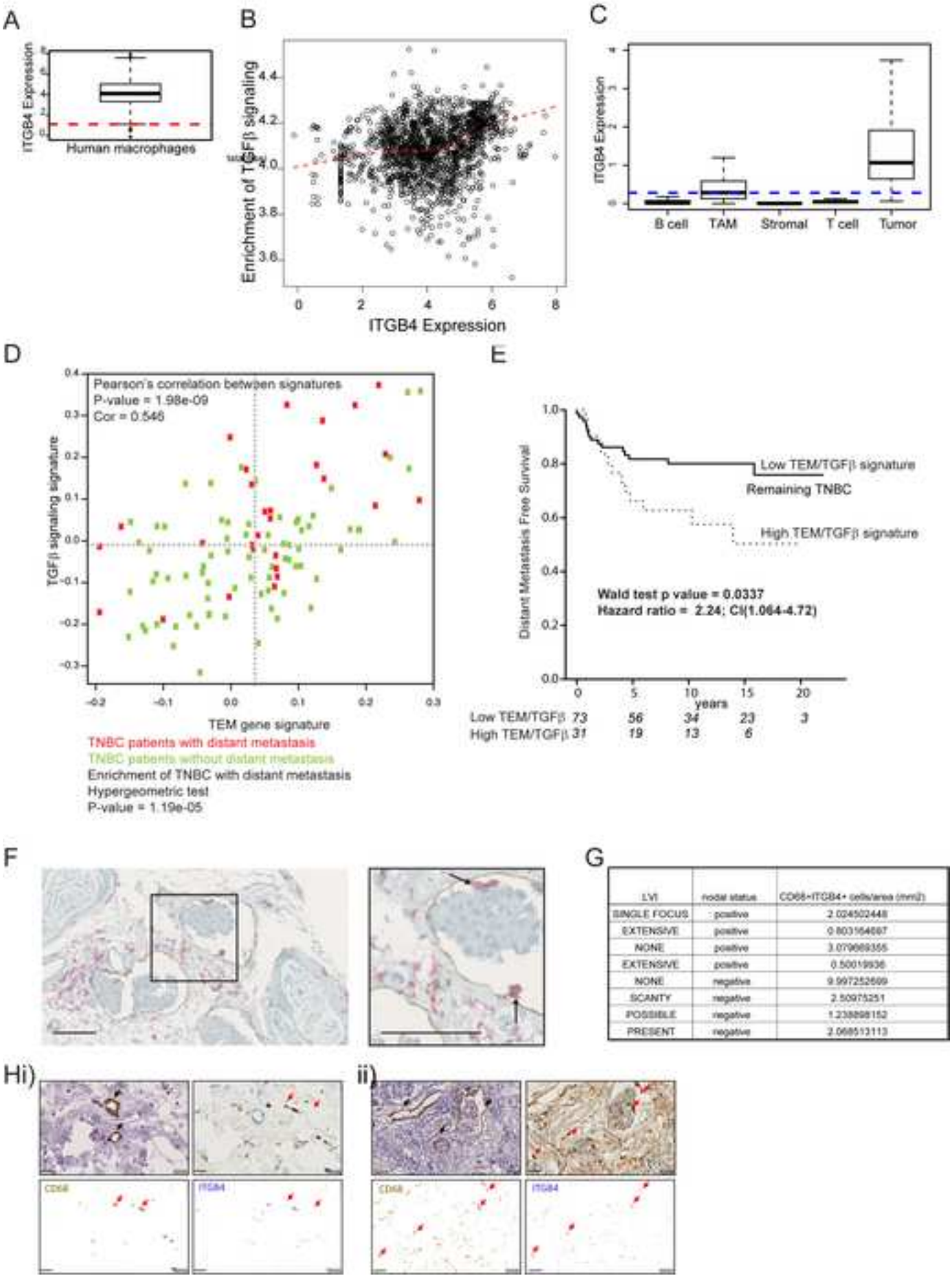

LVI	nodal status	CD68+ITGB4+ cells/area (mm2)
SINGLE FOCUS	positive	2.024502448
EXTENSIVE	positive	0.803154667
NONE	positive	3.079669355
EXTENSIVE	positive	0.50019936
NONE	negative	9.997252669
SCANTY	negative	2.50975251
POSSIBLE	negative	1.238898152
PRESENT	negative	2.068513113

Figure S1

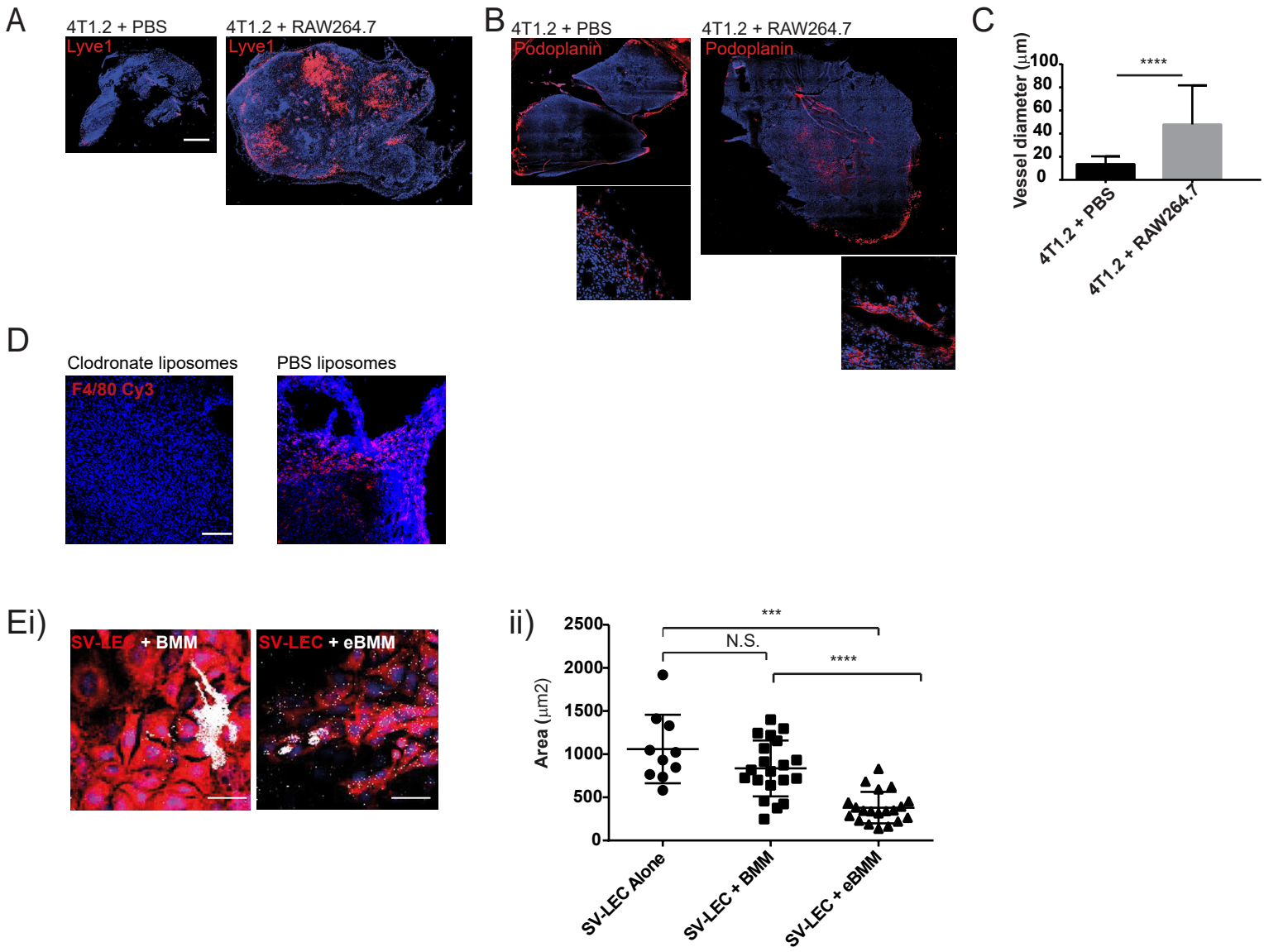

Figure S1. Elevated macrophages in tumor-bearing mice increases lymphatic vessel diameter and contact between SV-LEC and endogenous tumor-educated macrophages results in LEC contraction, related to Figure 2

Tile scans representative of whole tumor sections from mice treated with PBS or RAW264.7 macrophages.10 μm fixed sections were stained with (A) Lyve1 antibody and Cy3-conjugated secondary antibody or (B) podoplanin-AF594 (red) to allow confocal imaging of lymphatic vasculature i) (x4 objective, scale bar, 50 μm) (C) The maximum diameter across Lyve1+ vessels was measured in image J from at least 4 fields of view from each tumor section from 4 PBS-treated and 4 RAW264.7-treated mice. (D) Representative images of tumour tissues from mice treated with PBS liposomes or clodronate liposomes. F4/80-Cy3 (red) depicts infiltrating macrophages (E) SV-LECs were grown as a monolayer on a glass coverslip and stained with CMTMR (red) or CMFDA (green). Non-educated and tumor-educated bone marrow macrophages (BMM and eBMM respectively) were stained with F4/80-Cy5 (white) and both cell types were stained with Hoescht-33342 (blue).

Figure S2

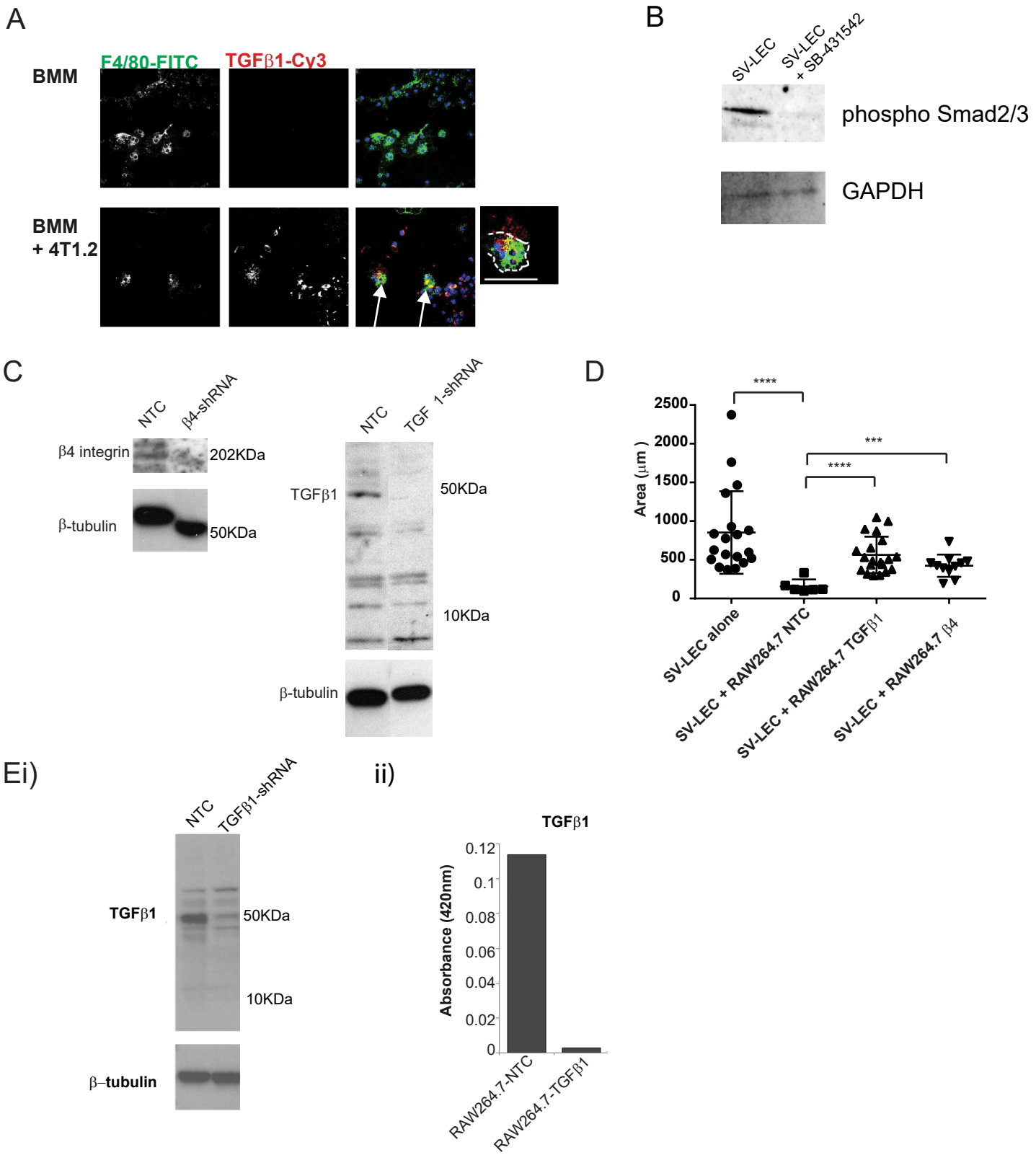

Figure S2. Western blot analysis of TGFβ1 knockdown in RAW264.7 cells, related to Figure 3
(A) Bone marrow macrophages were cocultured alone or with 4T1.2 tumor cells for 5 days on glass coverslips. Cells were fixed with 4% PFA before staining with F4/80-FITC and TGFβ1 and a Cy3 secondary antibody and imaging by confocal microscopy. Cell boundary depicted with white dotted line in inset image. (B) SV-LECs treated with SB-43142 were analysed by western blot to assess levels of phospho Smad2/3 (C) RAW264.7 were transiently transfected with shRNA against β4 integrin or TGFβ1 and analysed by western blot. (D) Macrophages were cocultured with SV-LECs and the contraction of SV-LECs measured (E) RAW264.7 cells were virally transduced with shRNA against TGFβ1 or NTC. (i) Macrophages that were transfected were selected for GFP expression and lysed using an SDS buffer. Lysates were run on a reducing gel (4-12% Bis-Tris), blotted onto PVDF and the membranes were probed for TGFβ1 or β-tubulin as a loading control. (ii) Supernatants were analysed by ELISA for TGFβ1 levels.

Figure S3

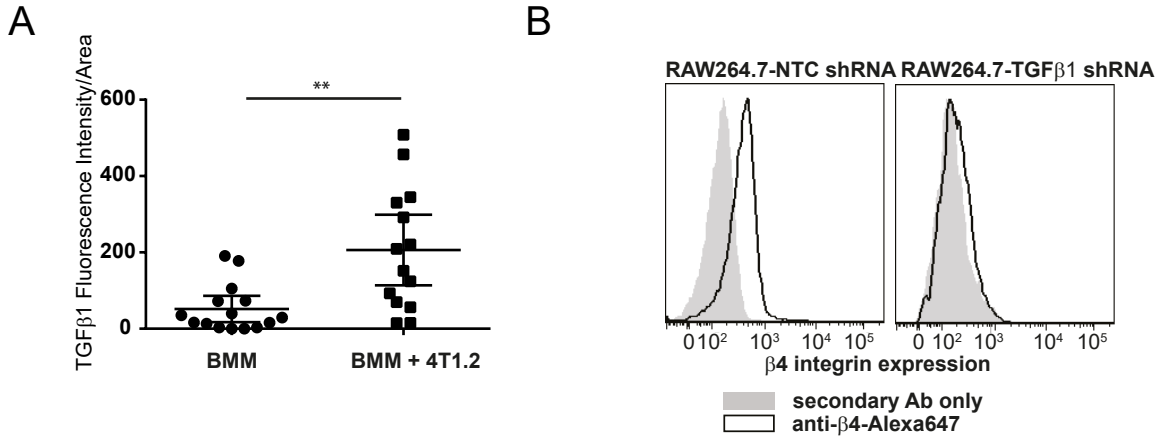

Figure S3. Endogenous macrophages increase expression of membrane-bound TGFβ1 after co-culture with 4T1.2 tumor cell, related to Figure 3

(A) The fluorescence intensity from F4/80+ cells was quantified (white arrows) and normalized to cell area. Scale bar, 10μm. Data represent means ± SD, significance was determined using unpaired t-tests (**p<0.01). (B) NTC- and TGFβ1-KD RAW264.7 macrophages were stained with rat anti-β4 integrin followed by secondary goat anti-rat-AF647 antibody. Expression levels of β4 integrin were analyzed by FACS and a representative histogram is depicted (n = 2 independent experiments).

Figure S4

A

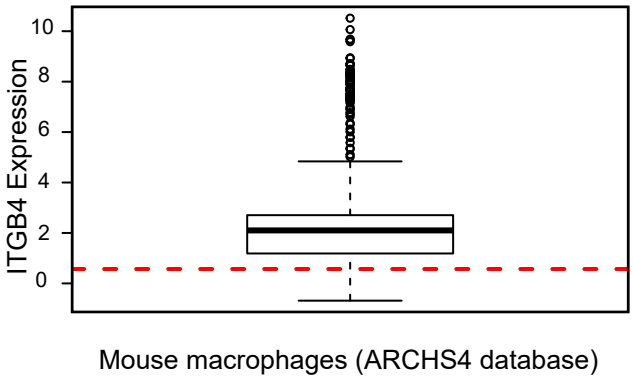

B

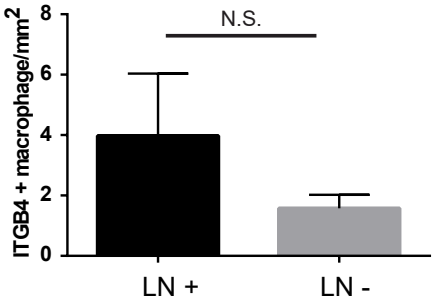

Figure S4. Expression of ITGB4 in murine macrophages (A) ITGB4 expression in murine macrophages, related to Figure 4

The y-axis indicates normalized expression on the log2 scale. The red line indicates median expression of all genes. Raw gene counts were obtained from the ARCHS4 database. (B) CD68+ITGB4+ macrophages in lymph node negative versus lymph node positive tissues are shown graphically.